Structurally Simple Supported Platinum Clusters Prepared from $[Pt_{15}(CO)_{30}]^{2-}$ on Magnesium Oxide

J.-R. Chang,[†] D. C. Koningsberger,[‡] and B. C. Gates*,[†]

Contribution from the Center for Catalytic Science and Technology, Department of Chemical Engineering, University of Delaware, Newark, Delaware 19716, and Laboratory for Inorganic Chemistry and Catalysis, Eindhoven University of Technology, 5600 MB Eindhoven, The Netherlands. *Received December 19, 1991*

Abstract: A Longoni-Chini cluster, $[Pt_{15}(CO)_{30}]^{2-}$, was prepared on MgO powder by a surface-mediated synthesis from Na_2PtCl_6 in the presence of CO. The formation of $[Pt_{15}(CO)_{30}]^{2-}$ and its decarbonylation at 120 °C under vacuum were characterized by infrared and X-ray absorption spectroscopies. The decarbonylated cluster had an average Pt-Pt bond distance of 2.76 Å and an average Pt-Pt first-shell coordination number of 3.7, indicating that the trigonal prismatic framework structure of the Longoni-Chini cluster was retained after decarbonylation; thus the decarbonylated cluster is represented as Pt_{15} with a trigonal prismatic structure. When this sample was recarbonylated, the Longoni-Chini cluster was not re-formed. The average Pt-Pt bond distance increased to 2.78 Å and the Pt-Pt first-shell coordination number increased to 6.0, indicating that a CO-induced morphology change gave approximately hemispherical Pt clusters with adsorbed CO.

Introduction

Structurally simple supported metals have been prepared from carbonyl clusters of Os,[1] Ir,[2] and a few other metals, but not yet from those of Pt. Pt is the most important catalytic metal, being applied for automobile exhaust conversion, naphtha reforming, and many other reactions. Preparation of structurally simple supported catalysts from Pt carbonyl clusters is difficult (1) because Pt carbonyls are highly air sensitive and difficult to synthesize in high yields on support surfaces and (2) because Pt easily forms metallic aggregates of various sizes and shapes. A recent report[3] of the high-yield synthesis of $[Pt_9(CO)_{18}]^{2-}$ and of $[Pt_{12}(CO)_{24}]^{2-}$ on the basic MgO surface and reports of simple decarbonylation of supported $[Os_{10}C(CO)_{24}]^{2-}$,[1] $[HIr_4(CO)_{11}]^-$,[2] and $[Ir_4(CO)_{12}]$[4] suggest that Pt cluster carbonyl anions could be formed on a basic support and decarbonylated without loss of cluster nuclearity.

Here we report the surface-mediated synthesis of $[Pt_{15}(CO)_{30}]^{2-}$ on MgO, its decarbonylation (without loss of nuclearity), and its recarbonylation (with changes in nuclearity). The surface structures have been characterized by infrared and X-ray absorption spectroscopies.

Results

Characterization of Surface and Extracted Species by Infrared and Ultraviolet-Visible Spectroscopy. The solid formed by deposition of Na_2PtCl_6 on MgO followed by treatment in CO was yellow-green. The surface species were characterized by infrared spectroscopy and by extraction into solution. The adsorbed species could not be extracted with neutral solvents such as THF, but extraction with [PPN][Cl] in THF was efficient, consistent with the occurrence of cation metathesis, which implies the presence of ionic species on the MgO surface. The yellow-green extract solution has infrared (Figure 1A) and ultraviolet-visible (Figure 2) spectra that are almost the same as those of $[Pt_{15}(CO)_{30}]^{2-}$ (Table I),[5-7] which is therefore identified as the organometallic species in the extract solution. The yield of $[Pt_{15}(CO)_{30}]^{2-}$ in the one-step extraction, estimated from the absorbance at 706 nm, was about 73%.

The ν_{CO} infrared spectrum of the surface species (Figure 1B) is almost the same as that of $[Pt_{15}(CO)_{30}]^{2-}$ in THF solution, except that another peak is present, at 1853 cm^{-1}. The comparison indicates that $[Pt_{15}(CO)_{30}]^{2-}$ was the predominant organometallic species on the MgO surface.

Decarbonylation and Recarbonylation of Pt Clusters on MgO. The infrared absorption bands of the platinum carbonyl species on MgO did not change in either intensity or position as the sample was heated under vacuum (0.01-0.001 Torr) to 65 °C (Figure 3A). The bridging CO band disappeared, and the intensity of the terminal CO absorption decreased to about one-third of the original value after 10 min at 75 °C under vacuum (Figure 3B). After 30 min at 75 °C, the intensity of the terminal CO band had decreased to about 10% of its original value (Figure 3C). The decarbonylation was complete after 30 min at 100 °C under vacuum (Figure 3D).

Table I. IR and UV-Visible Data for $[Pt_{15}(CO_{30})]^{2-}$ in Solutions and on Metal Oxide Supports

solvent or support	ν_{CO}, cm^{-1}	UV-visible absorption, nm	ref
THF	2055 vs, 1890 w, 1870 s, 1840 w, 1825 w		5
γ-Al_2O_3	2040 s, 1850 s		8
γ-Al_2O_3	2058 s, 1862 s		9
MgO	2059 s, 1877 s, 1853 s		this work
THF[a]	2055 vs, 1894 w, 1874 s, 1845 w		this work
acetonitrile		410, 700	6, 7
THF		406, 706	this work

[a] Species extracted from the solid following surface-mediated synthesis.

After the sample had been cooled to room temperature, CO (flowing at 50-100 mL/min at 1 atm) was introduced into the cell. A band assigned[3,8,9] to terminal CO ligands adsorbed on highly dispersed Pt clusters appeared at 2064 cm^{-1} (Figure 3E). The spectrum of $[Pt_{15}(CO)_{30}]^{2-}$ did not reappear.

X-ray Absorption Near Edge Structure (XANES). Pt L_{III} absorption edge data are shown in Figure 4 for the supported Pt sample formed by decarbonylation of $[Pt_{15}(CO)_{30}]^{2-}$ and for the sample formed by recarbonylation. The normalized L_{III} white-line intensity increased as a result of CO adsorption.

Extended X-ray Absorption Fine Structure (EXAFS) Reference Data. The EXAFS analysis for the supported Pt samples was based on phase shifts and backscattering amplitudes determined experimentally for materials of known crystal structure. The Pt-Pt

* Corresponding author.
[†] University of Delaware.
[‡] Eindhoven University of Technology.

(1) Lamb, H. H.; Krause, T. R.; Gates, B. C. *J. Chem. Soc., Chem. Commun.* **1986**, 821.
(2) Maloney, S. D.; van Zon, F. B. M.; Kelley, M. J.; Koningsberger, D. C.; Gates, B. C. *Catal. Lett.* **1990**, *5*, 161.
(3) Puga, J.; Patrini, R.; Sanchez, K. M.; Gates, B. C. *Inorg. Chem.* **1991**, *30*, 2479.
(4) van Zon, F. B. M.; Maloney, S. D.; Gates, B. C.; Koningsberger, D. C. To be published.
(5) Longoni, G.; Chini, P. *J. Am. Chem. Soc.* **1976**, *98*, 7225.
(6) Bhaduri, S.; Sharma, K. R. *J. Chem. Soc., Dalton Trans.* **1984**, 2309.
(7) Bhaduri, S.; Sharma, K. R. *J. Chem. Soc., Dalton Trans.* **1984**, 2315.
(8) Ichikawa, M. *Chem. Lett.* **1976**, 335.
(9) Handy, B. E.; Dumesic, J. A.; Langer, S. H. *J. Catal.* **1990**, *126*, 73.

0002-7863/92/1514-6460$03.00/0

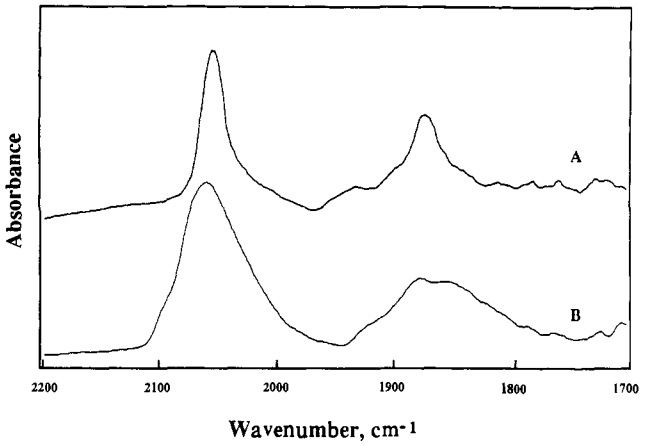

Figure 1. IR spectra of platinum carbonyl dianions prepared by a surface-mediated reductive carbonylation synthesis: A, species extracted from the MgO surface by ion exchange with [PPN][Cl] in THF; B, MgO-supported species.

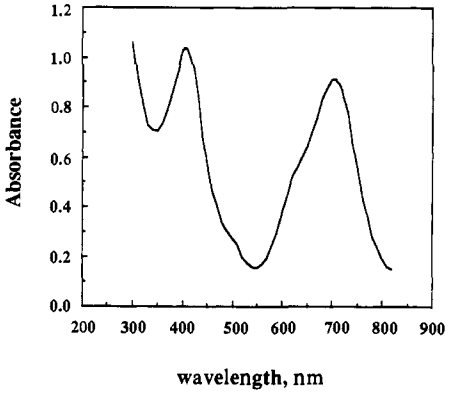

Figure 2. UV-visible spectrum of platinum carbonyl dianions extracted from the MgO surface by ion exchange with [PPN][Cl] in THF.

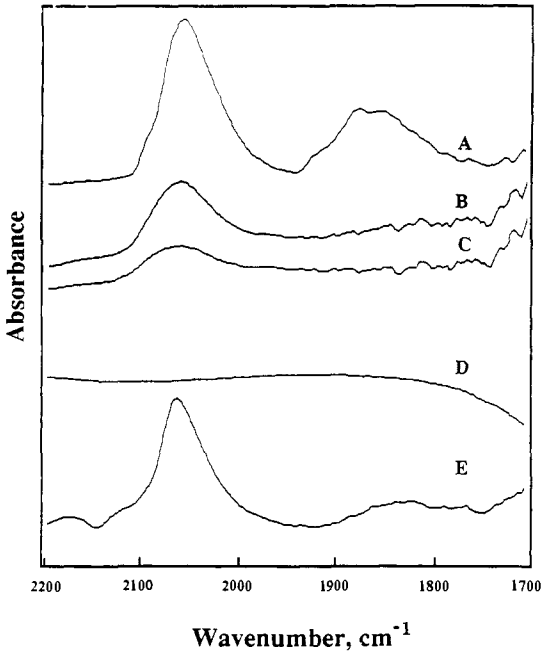

Figure 3. IR spectra of the MgO-supported species formed from $Na_2PtCl_6 \cdot 6H_2O$ by a surface-mediated reductive carbonylation synthesis: A, freshly prepared sample; B, sample after 10 min at 75 °C under vacuum (0.01–0.001 Torr); C, sample after 30 min at 75 °C under vacuum; D, sample after 30 min at 100 °C under vacuum; E, sample exposed to 1 atm of CO.

and $Pt-O_{support}$ contributions were analyzed with phase shifts and backscattering amplitudes obtained from EXAFS data for Pt foil and $Na_2Pt(OH)_6$, respectively. The Pt–C and Pt–O* interactions (where O* denotes the oxygen of a carbonyl ligand) were analyzed with phase shifts and backscattering amplitudes obtained from EXAFS data for crystalline $[Ir_4(CO)_{12}]$ (which has only terminal CO ligands) mixed with SiO_2. $[Ir_4(CO)_{12}]$ was chosen because the multiple-scattering effect in the Pt–O* shell is significant (as a consequence of the linear Ir–C–O* arrangement), and it was necessary to use a reference that exhibits multiple scattering.[10] The transferability of the phase shift and backscattering amplitudes for Pt and Ir has been justified both experimentally[12,13] and theoretically.[14] An IrAl alloy was used as a reference for the Pt–Mg absorber–scatterer pair because Al and Mg are nearby in the periodic table. Details of the preparation of the reference files are given elsewhere.[11] EXAFS parameters characteristic of the reference materials are summarized in Table II.

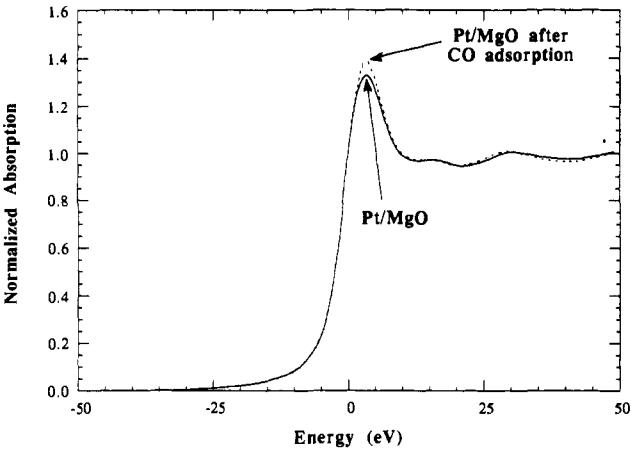

Figure 4. Structure of PtL_{III} absorption edge characterizing the supported Pt sample formed from the decarbonylation of the Pt carbonyl clusters on MgO at 120 °C: under vacuum (solid line); following CO treatment at 25 °C and 1 atm (dashed line).

Table II. Structural Parameters Characterizing Reference Materials Used in the EXAFS Analysis[a]

	crystallographic data[b]			Fourier transform data		
sample	shell	N	R, Å	Δk, Å^{-1}	Δr, Å	n
Pt foil	Pt–Pt[b]	12	2.77	1.9–19.8	1.9–3.0	3
$Na_2Pt(OH)_6$	Pt–O[c]	6	2.05	1.4–17.7	0.5–2.0	3
Ir–Al alloy	Ir–Al[d]	8	2.58	3.0–12.3	0.9–2.5	3
$Ir_4(CO)_{12}$	Ir–Ir	3	2.69			
	Ir–C[e]	3	1.87	2.8–16.5	1.1–2.0	3
	Ir–O*[e]	3	3.01	2.8–16.5	2.0–3.3	3

[a] Notation: N, coordination number for absorber–backscatterer pair; R, radial distance from crystal structure data; Δk limits used for forward Fourier transformation (k is the wave vector); Δr, limits used for shell isolation (r is distance); n, power of k used for Fourier transformation. [b] Crystal structure data from: Wyckoff, R. W. G. *Crystal Structures*, 2nd ed.; Wiley: New York, 1963; Vol. I, p 10. [c] Crystal structure data from: Trömel, M.; Lupprich, E. *Z. Anorg. Chem.* **1975**, *414*, 60. [d] Crystal structure data from: Esslinger, P.; Schubert, K. *Z. Metallkd.* **1957**, *48*, 126. After subtraction of the Ir–Ir contribution, $N = 3$, $R = 2.99$ Å, the Debye–Waller factor $\Delta\sigma^2 = 0.0033$ Å^2, and $E_0 = -3.5$ eV. [e] Crystal structure data from: Churchill, M. R.; Hutchinson, J. P. *Inorg. Chem.* **1978**, *17*, 3528. After subtraction of the Ir–Ir contribution, $N = 6$, $R = 2.69$ Å, $\Delta\sigma^2 = -0.001$ Å^2, and $E_0 = 2.5$ eV.

EXAFS Data and Preliminary Analysis. EXAFS data from two scans were averaged for each sample. The normalized EXAFS functions were obtained from the averaged X-ray absorption spectra by a cubic spline background subtraction and normalized

(10) Teo, B.-K. *J. Am. Chem. Soc.* **1981**, *103*, 3990.
(11) van Zon, F. B. M. Ph.D. Dissertation, Eindhoven University of Technology, Eindhoven, The Netherlands, 1988.
(12) Duivenvoorden, F. B. M.; Koningsberger, D. C.; Uh, Y. S.; Gates, B. C. *J. Am. Chem. Soc.* **1986**, *108*, 6254.
(13) Lengler, B. *J. Phys. (Paris)* **1986**, *47*, C8-75.
(14) Teo, B.-K.; Lee, P. A. *J. Am. Chem. Soc.* **1979**, *101*, 2815.

by division by the edge height.[11] The noise amplitude determined from the EXAFS averaging routine was about 0.001, and the signal amplitude at a value of k (k is the wave vector) of 4 Å^{-1} was about 0.04. These values give an estimated signal to noise ratio of 40/1. The k^3-weighted Pt–Pt phase- and amplitude-corrected Fourier transforms of the EXAFS functions in r space show that the amplitude of the major peak increased as a result of adsorption of CO, which implies that the Pt–Pt coordination number of the supported catalyst increased after CO adsorption. This inference is in need of further justification, however, because the major peak characteristic of the decarbonylated supported Pt sample contains only the Pt–Pt contribution, whereas both Pt–Pt and Pt–O* contributions characterize the sample after CO adsorption.

Detailed EXAFS Analysis for Decarbonylated $[Pt_{15}(CO)_{30}]^{2-}$ on MgO. A normal k^2-weighted Fourier transformation without correction was performed on the EXAFS data over the useful range ($3.51 < k < 13.84$ Å^{-1}). The major contributions were isolated by inverse Fourier transformation in the range $0.924 < r < 3.409$ Å. With the Koningsberger difference-file technique,[15,16] the Pt–Pt contribution, the largest component in the EXAFS spectrum, was estimated by calculating an EXAFS function that agreed as closely as possible with the experimental results in the high-k range ($7.5 < k < 13.5$ Å^{-1}); the metal–support contributions in this region are small. An EXAFS function calculated with the first-guess parameters was then subtracted from the data. The residual spectrum was expected to represent the metal–support interactions, including Pt–$O_{support}$ and Pt–Mg interactions. The difference file was estimated with two Pt–O contributions (a shorter[17-20] and a longer one[16,21-23]) first. As a first approximation, only four free parameters were estimated ($\Delta\sigma^2$, the Debye–Waller factor, and ΔE_0, the inner potential correction, were set equal to 0) to shorten the time for parameter estimation.

The first-guess Pt–Pt and Pt–$O_{support}$ contributions were then added and compared with the raw data in r space, and the fit was still not satisfactory. Then the Pt–$O_{support}$ contribution was subtracted from the data, and better parameters for the Pt–Pt contribution were estimated. The improved fit for the Pt–Pt contribution was subtracted from the data, and more accurate parameters for the contributions of the metal–support interface were determined by fitting the metal–support contributions to the residual spectrum with eight adjustable parameters; the initial guesses for parameter estimation were determined by adjusting the coordination parameters to give the best agreement with the residual spectrum, both in k space and in r space. This process was repeated, but even after many iterations, the fit was not good in the region $1.3 < r < 2.0$ Å. It was thus inferred that another contribution, Pt–Mg, had to be accounted for. A difference file was calculated by subtracting the best estimated Pt–Pt + Pt–$O_{support}$ contribution from the experimental EXAFS function. The Pt–Mg contribution was calculated by fitting the difference file with four adjustable parameters.

The Pt–Pt, Pt–Mg, and two Pt–$O_{support}$ contributions were then added, representing the overall fit of the data. To show the goodness of fit for both the high-Z (Pt) and low-Z (Mg, O) contributions, the raw data are compared with the fit, both in k space (with k^2 weighting) and in r space (with both k^1 and k^3 weighting) (Figure 5). The agreement is good. The structural parameters are shown in Table III. The number of parameters used to fit the data in this main-shell analysis is 16; the statistically justified number is approximately 17, estimated from the Nyquist theorem,[24] $n = (2(\Delta k)\Delta r/\pi) + 1$, where Δk and Δr, respectively,

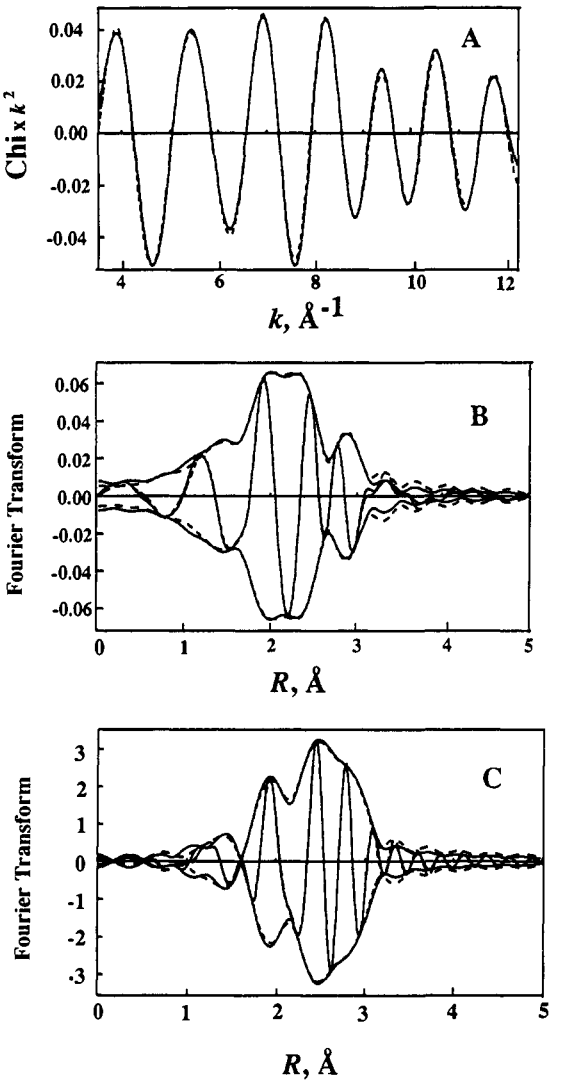

Figure 5. Results of EXAFS analysis obtained with the best calculated coordination parameters for the supported Pt sample prepared from the decarbonylation of the Pt carbonyl clusters on MgO at 120 °C under vacuum: A, EXAFS data (solid line) and sum of the calculated Pt–Pt + Pt–Mg + Pt–$O_{support}$ contributions (dashed line); B, imaginary part and magnitude of Fourier transform (k^3-weighted, Δk = 3.5–12.2 Å^{-1}) of EXAFS data (solid line) and sum of the calculated Pt–Pt + Pt–Mg + Pt–$O_{support}$ (Pt–O_l + Pt–O_s) contributions (dashed line); C, imaginary part and magnitude of Fourier transform (k^1-weighted, Δk = 3.5–12.2 Å^{-1}) of EXAFS data (solid line) and sum of the calculated Pt–Pt + Pt–Mg + Pt–$O_{support}$ contributions (dashed line).

Table III. EXAFS Results Characterizing the Surface Species Formed after Decarbonylation of $[Pt_{15}(CO)_{30}]^{2-}$ on MgO_{400}[a,b]

shell	N	R, Å	$\Delta\sigma^2$, Å^2	ΔE_0, eV	EXAFS ref
Pt–Pt	3.7	2.76	0.003 3	−0.87	Pt–Pt
Pt–$O_{support}$					
Pt–O_l	1.9	2.68	0.005 12	0.57	Pt–O
Pt–O_s	0.9	2.20	0.003 00	−3.0	
Pt–Mg	0.27	1.74	0.001 0	−4.0	Ir–Al

[a] Notation: N, coordination number for absorber–backscatter pair; R, radial distance; $\Delta\sigma^2$, Debye–Waller factor, difference with respect to reference compound; ΔE_0, inner potential correction (correction on the edge position); see ref 24 for details. [b] Estimated precision: N, ±15% (Pt–Mg, ±30%); R, ±1% (Pt–Mg, ±2%); $\Delta\sigma^2$, ±30%; ΔE_0, ±10%.

(15) Kirlin, P. S.; van Zon, F. B. M.; Koningsberger, D. C.; Gates, B. C. *J. Phys. Chem.* **1990**, *94*, 8439.
(16) van Zon, J. B. A. D.; Koningsberger, D. C.; van't Blik, H. F. J.; Sayers, D. E. *J. Chem. Phys.* **1985**, *82*, 5742.
(17) Emrich, R. J.; Mansour, A. N.; Sayers, D. E.; McMillan, S. T.; Katzer, J. R. *J. Phys. Chem.* **1985**, *89*, 4261.
(18) Lytle, F. W.; Greegor, R. B.; Marques, E. C.; Via, G. H.; Sinfelt, J. H. *J. Catal.* **1985**, *95*, 546.
(19) Via, G. H.; Sinfelt, J. H.; Lytle, F. W. *J. Chem. Phys.* **1979**, *71*, 690.
(20) Lagarde, P.; Murata, T.; Vlaic, G.; Freund, E.; Dexpert, H.; Bournonville, J. P. *J. Catal.* **1983**, *84*, 33.
(21) Koningsberger, D. C.; van Zon, J. B. A. D.; van't Blik, H. F. J.; Visser, G. J.; Prins, R.; Mansour, A. N.; Sayers, D. E.; Short, D. R.; Katzer, J. R. *J. Phys. Chem.* **1985**, *89*, 4075.
(22) Koningsberger, D. C.; Martens, J. H. A.; Prins, R.; Short, D. R.; Sayers, D. E. *J. Phys. Chem.* **1986**, *90*, 3047.
(23) Martens, J. H. Ph.D. Dissertation, Eindhoven University of Technology, Eindhoven, The Netherlands, 1988.

Table IV. EXAFS Results Characterizing the Surface Species Formed after CO Treatment of Pt Supported on MgO_{400}[a,b]

shell	N	R, Å	$\Delta\sigma^2$, Å^2	ΔE_0, eV	EXAFS ref
Pt–Pt	6.00	2.78	0.0041	−0.52	Pt–Pt
Pt–$O_{support}$					
Pt–O_l	0.58	2.78	0.0078	4.16	Pt–O
Pt–O_s	0.89	2.19	0.0047	−4.86	
Pt–CO					
Pt–C	0.82	1.86	0.0034	0.71	Ir–C
Pt–O*	0.77	2.99	0.0032	−3.72	Ir–O*

[a] Notation as in Table III. [b] Estimated precision: N, ±15% (Pt–O*, ±30%); R, ±1% (Pt–O*, Pt–C, Pt–O_l, and Pt–O_s, ±2%); $\Delta\sigma^2$, ±30%; ΔE_0, ±10%.

are the k and r ranges used in the forward and inverse Fourier transforms (Δk = 10.3 Å^{-1}; Δr = 2.483 Å).

Detailed Analysis for the Supported Pt Clusters after Recarbonylation. The data characterizing the sample after CO treatment were analyzed similarly. The EXAFS data were Fourier-transformed over the useful range (2.98 < k < 14.83 Å^{-1}) with k^2 weighting and no correction. The major contributions were isolated by inverse Fourier transformation in the range 0.482 < r < 3.250 Å. As before, the Pt–Pt contribution, the largest component in the EXAFS spectrum, was estimated first. However, since the Pt–O* contribution was strongly coupled with the Pt–Pt contribution, these two contributions had to be analyzed simultaneously. The structural parameters were estimated by fitting the data in the high-k range (7.5 < k < 14.5 Å^{-1}). The multiple scattering associated with Pt–C–O* groups was found to be significant in this range, with metal–support interface and Pt–C contributions being insignificant. Further analysis following the subtraction of the calculated Pt–Pt and Pt–O* contributions from the raw data led to characterization of the metal–support and the Pt–C contributions. The structural parameters characterizing these contributions were determined by fitting the residual spectrum with 12 parameters. The initial guesses for parameter estimation were again obtained by adjusting the coordination parameters to give the best fit of the residual spectrum in r space. The calculated Pt–C and Pt–$O_{support}$ contributions were subtracted from the raw data. Better parameters for the Pt–Pt and Pt–O* contributions were then estimated by fitting the residual spectrum. The refinement through this iteration was continued until good overall agreement was obtained. The final results are summarized in Table IV, and the comparisons of the data and the fit, both in k space and in r space, are shown in Figure 6. The number of parameters used to fit the data in this first-shell analysis is 20; the statistically justified number, calculated as above, is approximately 22.

Discussion

Synthesis of $[Pt_{15}(CO)_{30}]^{2-}$ on the MgO Surface. The results are consistent with the conclusion that $PtCl_6^{2-}$ on the MgO surface was converted into $[Pt_{15}(CO)_{30}]^{2-}$ in the presence of CO. The extraction of this anion into solution confirms that it was present on the surface, and the color and infrared spectra of the solid are consistent with the inference that this anion was the predominant organometallic species on the surface. The infrared spectrum of the surface species (2059 s, 1877 s, 1853 s cm^{-1}) is indistinguishable from that of $[Pt_{15}(CO)_{30}]^{2-}$ in THF solution, except for the additional peak at 1853 cm^{-1}. This peak is characteristic of bridging CO ligands, with the shift to lower energy suggested to be a consequence of interactions of such ligands with Lewis acid sites (Mg^{2+}) on the MgO surface. Similar results have been reported by Handy et al.,[9] who adsorbed the PPN salt of $[Pt_{15}(CO)_{30}]^{2-}$ onto γ-Al_2O_3; they observed infrared peaks at 2058 and 1862 cm^{-1}.

The synthesis of $[Pt_{15}(CO)_{30}]^{2-}$ on the basic MgO surface is consistent both with the chemistry of platinum carbonyls in basic solutions, reported by Longoni and Chini,[5] and with the surface chemistry reported by Puga et al.,[3] who formed $[Pt_9(CO)_{18}]^{2-}$ and, separately, $[Pt_{12}(CO)_{24}]^{2-}$ on MgO. The surface-mediated synthesis reported here is simple and gives $[Pt_{15}(CO)_{30}]^{2-}$ in high yield (>73%, based on a single extraction with [PPN][Cl]). The method is evidently more effective than that reported by Puga et al.,[3] as indicated by the more precise agreement in this work than in Puga's of the spectrum of the extracted platinum cluster anion with that of the pure anion in solution. The method used here is almost the same as Puga's; the improvement is attributed to the minimization of the surface contamination by traces of air in this work; the solvent (methanol or hexane) evidently protected the platinum complex by providing resistance to mass transfer of oxygen. The method reported here also gives higher yields of $[Pt_9(CO)_{18}]^{2-}$ than Puga's method.

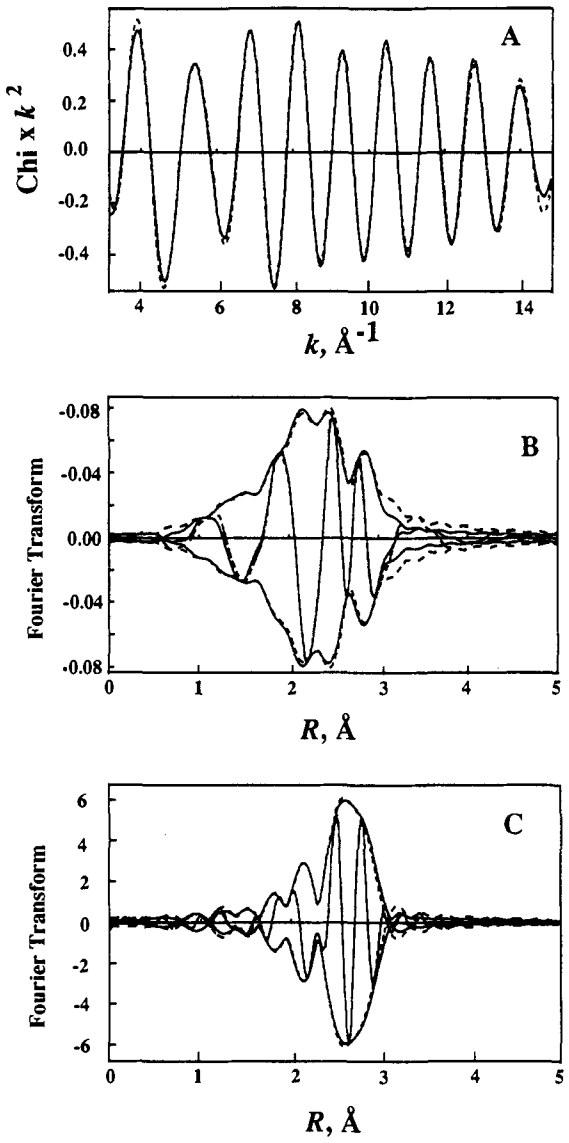

Figure 6. Results of EXAFS analysis obtained with the best calculated coordination parameters for the supported Pt sample prepared from the decarbonylation of the Pt carbonyl clusters on MgO at 120 °C under vacuum, followed by CO treatment at 25 °C and 1 atm: A, EXAFS data (solid line) and sum of the calculated Pt–Pt + Pt–Mg + Pt–$O_{support}$ contributions (dashed line); B, imaginary part and magnitude of Fourier transform (k^3-weighted, Δk = 3.00–14.8 Å^{-1}) of EXAFS data (solid line) and sum of the calculated Pt–Pt + Pt–Mg + Pt–$O_{support}$ (Pt–O_l + Pt–O_s) contributions (dashed line); C, imaginary part and magnitude of Fourier transform (k^1-weighted, Δk = 3.00–14.8 Å^{-1}) of EXAFS data (solid line) and sum of the calculated Pt–Pt + Pt–Mg + Pt–$O_{support}$ contributions (dashed line).

Decarbonylation of $[Pt_{15}(CO)_{30}]^{2-}$ Supported on MgO. The decarbonylation of $[Pt_{15}(CO)_{30}]^{2-}$ on MgO was carried out under vacuum by gradually increasing the temperature. Both terminal

(24) Koningsberger, D. C.; Prins, R. *X-ray Absorption: Principles, Applications, Techniques of EXAFS, SEXAFS and XANES*; Wiley: New York, 1988; p 395.

and bridging absorption bands decreased in intensity as the temperature was increased. The peaks at 1877 and 1853 cm^{-1} (indicating bridging CO) decreased in intensity faster than the peak at 2059 cm^{-1} (indicating terminal CO). These results suggest that the bridging CO ligands are more labile than the terminal ligands and are consistent with the work of Handy et al.[9] However, in Handy's work, both the terminal and bridging bands shifted to lower energy as the degree of decarbonylation increased; such a result was not observed in this work. The reasons for the difference may be related to the difference in the decarbonylation environment; our sample was evacuated, but Handy's was treated in He and presumably contained residual CO, which may have readsorbed on the metal, with the amount decreasing with increasing temperature. The decrease of CO coverage leads to diminished dipole–dipole coupling between adjacent CO molecules and a lower energy shift of the CO absorption bands.[25,26]

To investigate the structure of the clusters resulting from the decarbonylation, the sample was characterized by EXAFS spectroscopy. The Pt–Pt coordination number characteristic of the sample prepared by decarbonylation of $[Pt_{15}(CO)_{30}]^{2-}$ on MgO (Table III), 3.7, is nearly the same as the crystallographically determined Pt–Pt coordination number[5] of $[Pt_{15}(CO)_{30}]^{2-}$ (3.6). This result suggests that the structure of the Pt cluster frame after decarbonylation resembles that of the trigonal prism of $[Pt_{15}(CO)_{30}]^{2-}$. This suggestion is consistent with infrared spectra and the EXAFS results characterizing the metal–support interface (Table III) as follows: There was no significant band shift or peak splitting observed in the infrared spectra recorded during the decarbonylation of $[Pt_{15}(CO)_{30}]^{2-}$ on MgO, which implies that no detectable Pt carbonyl clusters formed as intermediates. The only possible structure of a Pt_{15} cluster with a Pt–Pt coordination number of 3.7 is rodlike. The coordination number characterizing the metal–support interface, namely, 2.8 (Pt–O_s + Pt–O_l) (where s refers to the short and l to the long Pt–O distance), is close to 2.67, which is the value expected for a trigonal prism of Pt atoms on the (100) face of MgO, which is the most stable (and predominant) face of MgO.[27] Other plausible structures, such as a square prism, have metal–support coordination numbers less than 2.0 and are ruled out. In summary, all the data are consistent with a trigonal prism, and we regard this structure as an appropriate model of the decarbonylated Pt clusters. The model is simplified, as there may be a variety of structures rather than just one, and as the MgO support surface is inherently nonuniform.

Recarbonylation of the Supported Pt Clusters. After the MgO-supported $[Pt_{15}(CO)_{30}]^{2-}$ had been decarbonylated and cooled to room temperature, it was exposed to flowing CO at 1 atm in an attempt to regenerate the Pt carbonyl clusters. A terminal CO absorption band with about 70% of the intensity of that characterizing the original $[Pt_{15}(CO)_{30}]^{2-}$ appeared at 2064 cm^{-1}, but the bridging CO peaks did not reappear. These results are consistent with those of Handy et al.,[9] who observed that only a terminal CO peak at 2072 cm^{-1} reappeared upon recarbonylation of the sample prepared from the deposited salt of $[Pt_{15}(CO)_{30}]^{2-}$. The results show that the original Pt carbonyl clusters were not regenerated after CO readsorption.

After CO treatment of the decarbonylated sample, the Pt–Pt first-shell coordination number increased from 3.7 to 6.0, and the Pt–O (Pt–O_s + Pt–O_l) coordination number decreased from 2.8 to 1.4 (Tables III and IV), indicating the increased size of the Pt clusters. A further characterization of the structure of these Pt clusters is provided by the higher metal–metal shell contributions. According to the report of van Zon et al.,[4] small supported Ir clusters assumed to have a face centered cubic structure on a (100) basal plane of MgO showed a high amplitude of the second metal–metal shell, consistent with nearly hemispherical clusters. The increase in the intensity of the Pt–Pt higher-shell contribution observed in this work as a result of recarbonylation (Figure 6) indicates a change in the morphology of the clusters from that resembling trigonal prisms to that resembling hemispheres. The average clusters changed from about 1.5 nm long trigonal prisms to hemispheres with a diameter of about 1.0 nm. The average Pt–Pt bond distance increased from 2.76 to 2.78 Å, and the Debye–Waller factor increased slightly (indicating a small increase in the dispersion of Pt–Pt distances). The increases in the average Pt–Pt distance and in the Debye–Waller factor are small (within experimental error) and are not conclusive evidence, but they are consistent with the growth of the Pt clusters upon CO adsorption. Several groups have observed lengthening of the metal–metal bond distance with the growth of supported metal clusters.[28–30]

The intensity of the threshold resonance of the L_{III} absorption edge (white line) is related to the transition probabilities of exciting inner-core 2p electrons into vacant d valance levels. The lower the electron density of the metal, the greater the number of vacancies in the valence level and, hence, the higher the probability of the transition.[31] The effect of CO adsorption on the d-hole density of Pt can thus be inferred from the white-line intensity. However, a correction of white-line intensities to account for the influence of the metal cluster size is needed.

Hartree–Fock–Slater LCAO calculations show a decrease of the d-hole density with increasing size of ionized clusters.[32] The result is consistent with XANES experiments; the white-line intensity of supported metal clusters decreases with increasing cluster size, and the XANES spectrum is computed by considering scattering of the electron in the field of the ionized cluster.[33]

From the EXAFS results, it was at first expected that the white-line intensity would decrease after CO adsorption because of the growth of the Pt clusters. However, the reverse was observed. The observation is explained by a decrease in the electron density of the Pt clusters. This result is consistent with the infrared results. When CO is adsorbed on the Pt clusters, electron transfer occurs from the d orbitals of Pt to the antibonding π^* orbitals of CO, leading to a lowering of Pt electron density and the CO absorption frequency (from 2143 cm^{-1}, characteristic of CO gas, to 2064 cm^{-1}, characteristic of carbonyl ligands).[34]

CO adsorption is a common characterization technique used to determine the dispersion (fraction of the metal atoms exposed) of supported metal catalysts.[35] The present results indicate that CO is not always an innocent adsorbate. Depending on the metal cluster size and hydroxyl group content of the support surface, CO may induce significant morphological changes in the metal, leading to inaccuracy of the dispersion measurements. The adsorption of CO on highly dispersed supported Rh, Ir, and Ru catalysts has been reported to lead to the disruption of the metal clusters, and the surface hydroxyl groups play a principal role. The reaction is described as oxidative fragmentation, and the process can be formulated in a simplified way as follows:[36–41]

$$(1/x)M_x + \{Al\text{–}OH\} + 2CO(g) \rightarrow \{Al\text{–}O\}M(CO)_2 + \tfrac{1}{2}H_2 \quad (1)$$

where M represents Rh, Ir, or Ru and the braces refer to groups terminating an aluminum oxide surface.

(25) Primet, M.; Basset, J.-M.; Mathieu, M. V.; Prettre, M. *J. Catal.* **1973**, *29*, 213.
(26) Primet, M. *J. Catal.* **1984**, *88*, 273.
(27) Henrich, V. C. *Rep. Prog. Phys.* **1985**, *48*, 1481.
(28) Balerna, A.; Bernieri, E.; Picozzi, P.; Reale, A.; Santucci, S.; Burattini, E.; Mobilio, S. *Phys. Rev.* **1985**, *B31*, 5058.
(29) van't Blik, H. F. J.; von Zon, J. B. A. D.; Koningsberger, D. C. *J. Mol. Catal.* **1984**, *25*, 379.
(30) Balerna, A.; Mobilio, S. *Phys. Rev.* **1986**, *B34*, 2239.
(31) Lytle, F. W.; Wei, P. S. P.; Greegor, R. B.; Via, G. H.; Sinfelt, J. H. *J. Chem. Phys.* **1979**, *70*, 4849.
(32) Koningsberger, D. C. To be published.
(33) Ravenek, W.; Jansen, A. P. J.; van Santen, R. A. *J. Phys. Chem.* **1989**, *93*, 6445.
(34) Cotton, F. A.; Wilkinson, G. *Advanced Inorganic Chemistry*; Wiley: New York, 1988; p 61.
(35) Anderson, R. B., Dawson, P. T., Eds. *Experimental Methods in Catalytic Research*; Academic Press: New York, 1976; Vol. 2.
(36) Cavanagh, R. R.; Yates, J. T., Jr. *J. Chem. Phys.* **1981**, *74*, 4150.
(37) van't Blik, H. F. J.; van Zon, J. B. A. D.; Huizinga, T.; Vis, J. C.; Koningsberger, D. C.; Prins, R. *J. Am. Chem. Soc.* **1985**, *107*, 3139.
(38) Solymosi, F.; Novak, E.; Molnar, A. *J. Phys. Chem.* **1990**, *94*, 7250.
(39) Solymosi, F.; Rasko, J. *J. Catal.* **1989**, *115*, 107.
(40) Paul, D. K.; Yates, J. T., Jr. *J. Phys. Chem.* **1991**, *95*, 1699.
(41) Ballinger, T. H.; Yates, J. T., Jr. *J. Phys. Chem.* **1991**, *95*, 1694.

In contrast to Rh, Ir, and Ru cases, no cluster disintegration has been observed for Pd as a result of CO adsorption. Instead, larger clusters have been formed,[42,43] as observed here for Pt. The details of the chemistry whereby CO adsorption causes Pt cluster aggregation remain to be elucidated. Our observations and the published results[43] suggest a role of surface hydroxyl groups.

The interaction between metal clusters and surface oxygen has been investigated by Lytle et al.[18] The characteristic interaction between the metal and hydroxyl groups was characterized theoretically by Martens[23] and experimentally by Koningsberger et al.[21,22] The interaction between metal and surface hydroxyl groups is thermodynamically quite unstable; EXAFS results demonstrate that the evacuation[44] of a reduced $Ir/\gamma\text{-}Al_2O_3$ sample at 350 °C leads to removal of OH groups from the metal–support interface, resulting in the disappearance of the long metal–support distance, accompanied by a structural rearrangement of the metal–support interface. Similarly, after CO treatment of the reduced supported Pt clusters, the coordination number of the long Pt–O distance decreases, whereas that of the short Pt–O distance is unchanged (Tables III and IV).

These results provide a confirmation of the inference that the interactions between metal clusters and surface hydroxyl groups are weak. CO molecules may replace the hydroxyl groups bonded to Pt, or the surface energy of Pt clusters may be modified by CO, resulting in a weakening of the interaction between Pt and surface hydroxyl groups.

Therefore, on the basis of the EXAFS results (Tables III and IV), the decarbonylation of Pt carbonyl clusters on MgO at 120 °C under vacuum and their recarbonylation are formulated very roughly as follows:

$$[Pt_{15}(CO)_{30}]^{2-} \xrightarrow{MgO} Pt_{15}\{HOMg\}_{30}\{OMg\}_{15} + 30CO \quad (2)$$

$$(x/15)Pt_{15}\{HOMg\}_{30}\{OMg\}_{15} + 0.75xCO \rightarrow Pt_x(CO)_{0.75x}\{HOMg\}_{0.5x}\{OMg\}_x \quad (3)$$

Where {OMg} and {HOMg} represent the oxygen ions and hydroxyl groups of the MgO surface that interact with Pt clusters at distances of about 2.1–2.2 and 2.7–2.8 Å, respectively.

In summary, we might speculate on the mechanism from the evidence that the metal–support interaction decreases after CO adsorption and the Pt clusters tend to coalesce. Since the affinity of Pt for CO is greater than that for {HOMg} groups, CO ligands may replace {HOMg} and loosen the interaction of the Pt atoms with the support. After the formation of Pt carbonyl species, the affinity of a mobile Pt carbonyl species for other Pt carbonyl species may be greater than that of Pt carbonyl species for the support. Consequently, a more stable morphology, characterized by larger, nearly hemispherical (and nonuniform) Pt clusters, may result. In contrast, the carbonyls of the less noble (more oxophilic) Rh, Ir, and Ru have greater affinity for the metal oxide support than Pt carbonyls do. Instead of agglomeration to give zerovalent metal clusters, the oxidative disruption of the clusters takes place, giving cationic metal complexes with surface O^{2-} ions and/or OH^- groups as ligands.

Experimental Methods

Materials and Sample Preparation. Sample preparation and handling were carried out with exclusion of air and moisture on a double-manifold Schlenk vacuum line or in a nitrogen-filled Braun glovebox in which the concentrations of O_2 and water were typically less than 1.0 and 0.1 ppm, respectively. The solvents were dried and deoxygenated prior to use; THF and hexane were dried over sodium benzophenone ketyl, and methanol was dehydrated by distillation from Mg and sublimed I_2. The MgO support (EM Science) was pretreated by heating to 400 °C in flowing O_2 (Matheson, extra dry grade) for 4 h, followed by evacuation for 8 h. The surface area was approximately 75 m^2/g. To make the supported platinum, $[Na]_2[PtCl_6]$ (Aesar, 99.9%), used without further purification, was added to a methanol (50 mL) slurry of pretreated MgO powder (3 g) at room temperature. The amounts were chosen so that adsorption of all the $[Na]_2[PtCl_6]$ by the MgO would have given a solid containing 2 wt % Pt. After the reaction mixture was stirred under CO (Matheson, 99.99%) at room temperature for 8 h, a yellow-green color was observed in both the liquid and solid phases. The methanol solvent was pumped off under vacuum for 6 h at room temperature. The resultant yellow-green solid was transferred to the drybox for storage, and the infrared spectrum was immediately recorded.

Characterization of Extracted Surface Species by IR and UV–Visible Spectroscopy. Extraction of the surface organometallic species was performed in a CO environment with a saturated solution of bis(triphenylphosphoranylidene)ammonium chloride, [PPN][Cl] (Strem, 99.9%). One gram of the sample was loaded into a Schlenk flask in a drybox. The species formed on the MgO surface were extracted under an atmosphere of CO by addition of approximately 60 mL of [PPN][Cl] in a THF solution. Solution IR spectra were recorded with a Nicolet 510M spectrometer with a spectral resolution of 4 cm^{-1}. The extracted solution was further diluted to about $^1/_{40}$th of its original concentration. Solution UV–visible spectra were measured with a Hewlett-Packard 8425 spectrometer. The IR and UV–visible cells were designed to exclude air and moisture.

Characterization of Surface Species by DRIFTS. Diffuse reflectance infrared Fourier transform spectra (DRIFTS) of surface species were recorded with the Nicolet 510M instrument. The powder samples were loaded into the DRIFTS cell in the drybox. The cell was connected to a vacuum/gas-handling manifold for in-situ treatment.[45] The decarbonylation of the sample was carried out in the cell under vacuum (0.01–0.001 Torr). The temperature was increased at about 5 °C/min in intervals of 25 °C and maintained for 30 min, until finally at 100 °C no significant peaks remained in the carbonyl stretching range, 1700–2200 cm^{-1}. After this decarbonylation, the sample was cooled to room temperature. CO (flowing at 50–100 mL/min at 1 atm) was then introduced into the cell, and its flow was maintained for about 20 min. After the CO treatment, the cell was evacuated to a pressure of approximately 10^{-2}–10^{-3} Torr, and IR spectra were again recorded.

EXAFS Spectroscopy. The EXAFS experiments were performed on X-ray beamline X-11A at the National Synchrotron Light Source at Brookhaven National Laboratory, Upton, Long Island, NY. The ring energy was 2.5 GeV and the ring current 60–200 mA. The Si(111) channel-cut monochromator was detuned 20% to reject higher harmonics; resolution, $\Delta E/E$, was 2.0×10^{-4}. The EXAFS spectra were recorded with the sample in a cell that allowed treatment under vacuum or in flowing gases prior to the measurements. The powder samples were pressed into wafers in a N_2-filled glovebag with the wafer thickness chosen to give an absorbance of 2.5. The EXAFS measurements were made in the region of the $Pt L_{III}$ edge with the cell cooled by liquid N_2.

The supported Pt sample was prepared by decarbonylation of the initially prepared platinum carbonyl at 120 °C for 1 h under vacuum (0.01–0.001 Torr). The sample was loaded into the EXAFS cell in a N_2-filled glovebag and then scanned twice in the N_2 environment. After data collection, the cell was allowed to warm to room temperature, and flow of CO (50–100 mL/min at 1 atm) was started and maintained for 0.5 h. Then the cell was evacuated (0.01 Torr) and cooled to liquid nitrogen temperature, and the EXAFS spectrum was again recorded. EXAFS data for the reference materials, Pt foil, $Na_2Pt(OH)_6$, Ir–Al alloy, and $[Ir_4(CO)_{12}]$, were measured as described separately.[11]

Conclusions

Surface-mediated synthesis was used to prepare $[Pt_{15}(CO)_{30}]^{2-}$ on the surface of MgO powder. The bridging CO ligands of this supported cluster are more labile than the terminal CO ligands, and decarbonylation under vacuum commenced with the removal of the bridging CO ligands at 75 °C, followed by the removal of the terminal CO ligands at 100 °C. The decarbonylated Pt cluster is modeled as a trigonal prism to account for the EXAFS data. Readsorption of CO did not regenerate the original $[Pt_{15}(CO)_{30}]^{2-}$; rather, it induced Pt cluster growth to give nonuniform structures resembling hemispheres.

Acknowledgment. We gratefully acknowledge the support of the National Science Foundation (Grant CTS-9012910); we also acknowledge the U.S. Department of Energy, Division of Materials Science, under Contract No. DE-FG05-89ER45384, for its role in the operation and development of Beamline X-11A at the National Synchrotron Light Source. The NSLS is supported by

(42) Zhang, Z.; Chen, H.; Sheu, L.-K.; Sachtler, W. M. H. *J. Catal.* **1991**, *127*, 213.
(43) Anderson, S. L.; Mizushima, T.; Udagawa, Y. *J. Phys. Chem.* **1991**, *95*, 6603.
(44) Kampers, F. W. H.; Koningsberger, D. C. *Faraday Discuss. Chem. Soc.* **1990**, *89*, 137.
(45) Zhou, P.-L.; Maloney, S. D.; Gates, B. C. *J. Catal.* **1991**, *129*, 315.

the Department of Energy, Division of Materials Science and Division of Chemical Sciences, under Contract No. DE-AC02-76CH00016. The international collaboration was supported by a NATO travel grant.

Supplementary Material Available: Figures showing raw EXAFS data and additional plots giving details of the EXAFS analysis (7 pages). Ordering information is given on any current masthead page.

A Test of the Utility of Plane Waves for the Study of Molecules from First Principles

Andrew M. Rappe,[†] J. D. Joannopoulos,[†] and P. A. Bash*[,‡]

Contribution from the Department of Physics and Chemistry and the Research Laboratory of Electronics, Massachusetts Institute of Technology, Cambridge, Massachusetts 02139, and Department of Chemistry, Florida State University, Tallahassee, Florida 32306.
Received August 19, 1991

Abstract: This paper studies the applicability of a plane-wave basis set for density functional calculations of the properties of molecules from first principles. The main features of the plane-wave method are described, including pseudopotentials and supercells. The results for a number of small molecules are reported. The close agreement with experiment and with a standard method of quantum chemistry calculation indicates the promise which this method holds for chemical and biochemical first-principles computations.

I. Introduction

Density functional theory[1,2] has recently shown significant promise[3,4] as an analytical tool for studying chemical systems from first principles. Currently, the calculations of properties of molecules containing first-row elements are most commonly performed using a basis set of localized orbitals for wave function expansions. The purpose of this paper is to report results which indicate the viability of the plane-wave basis set as an alternative choice for this expansion. First we will describe the salient features of this computational method, and then we will exhibit structural results for a number of small molecules.

The plane-wave basis set has a number of extremely desirable features. The set of plane waves is complete and orthonormal. In addition, plane waves can be indexed by a single vector index, the wave vector. These two properties make finite sets of plane waves systematically improvable in a straightforward manner. A calculation is performed using a basis set of all plane waves such that each plane wave's wave vector has a magnitude less than some value, the plane-wave cutoff. Then the basis set is improved by increasing the plane-wave cutoff until the results converge.[5,6] This systematic improvability provides another advantage, the numerical stability of results. Another benefit of using plane waves is that a priori knowledge of the electronic distribution is not required for the generation of the basis set. Finally, there are reliable and efficient methods for finding electronic eigenstates and atomic positions. The Car and Parrinello molecular dynamics method,[7,8] because it allows simultaneous updates to wave functions and atoms, speeds up calculations significantly relative to traditional matrix diagonalization approaches. The fast Fourier transform algorithm improves the scaling of many parts of the calculation, and the conjugate gradient technique[9,10] for minimizing the electronic energy makes possible the study of large molecules, whereas other minimization techniques exhibit instability as the cell size becomes very large. The scaling behavior of the various parts of the calculation is shown in Table I. A gauge of the computational time for this method is the time required to calculate the total energy and quantum-mechanical forces on the ions in a particular geometry. For the formamide molecule in a 7-Å box with a plane-wave cutoff of 544.232 eV (40 Ry), this calculation requires approximately 450 CPU s on a Cray-2 computer.

Table I. Scaling Properties of the LDAP-PW Method[a]

step	scaling
Fourier transform of wave functions	$N_b N_{pw} \ln (N_{pw})$
acceleration of coefficients	$N_b N_{pw} \ln (N_{pw})$
forces on ions	$N_b N_i N_{pw}$
orthogonalization	$N_b N_b N_{pw}$

[a] N_b is the number of filled bands (orbitals), N_i is the number of ions, and N_{pw} is the number of plane waves. N_{pw} is roughly 100 times larger than N_b, which is twice the size of N_i.

The chief difficulty with using plane waves as a basis set is that sharply-peaked functions require huge numbers of plane waves to converge. For this reason, expression of core electrons using plane waves is extremely difficult. Because valence electrons are orthogonalized to the core, even the expression of valence electrons is very difficult when core electrons are included in the calculation. This problem has been surmounted by the use of pseudopotentials.[11,12] A pseudopotential is a weaker potential than the Coulomb potential, and it includes the effects of the core electrons implicitly. To generate a pseudopotential, a density functional calculation is normally performed on a free atom with specified electron fillings of the orbitals. A pseudopotential is then con-

[†] Massachusetts Institute of Technology.
[‡] Florida State University.

(1) Hohenberg, P.; Kohn, W. *Phys. Rev.* **1964**, *136*, B864.
(2) Kohn, W.; Sham, L. J. *Phys. Rev.* **1965**, *140*, A1133.
(3) For a current survey, see: *Density Functional Methods in Chemistry*; Springer-Verlag: New York, 1991.
(4) Parr, R. G.; Yang, W. *Density Functional Theory of Atoms and Molecules*; Oxford: New York, 1989.
(5) Ihm, J.; Zunger, A.; Cohen, M. L. *J. Phys. C.: Solid State Phys.* **1979**, *12*, 4409.
(6) For reviews, see: Joannopoulos, J. D. In *Physics of Disordered Materials*; Plenum Publishing: New York, 1985. Pickett, W. *Comput. Phys. Rep.* **1989**, *9*, 115.
(7) Car, R.; Parrinello, M. *Phys. Rev. Lett.* **1985**, *55*, 2471.
(8) Payne, M. C.; Joannopoulos, J. D.; Allan, D. C.; Teter, M. P.; Vanderbilt, D. H. *Phys. Rev. Lett.* **1986**, *56*, 2656.
(9) Teter, M. P.; Payne, M. C.; Allan, D. C. *Phys. Rev. B* **1989**, *40*, 12255.
(10) Arias, T. A.; Payne, M. C.; Joannopoulos, J. D. *Phys. Rev. B* **1992**, *45*, 1538.
(11) Phillips, J. C. *Phys. Rev.* **1958**, *112*, 685.
(12) Cohen, M. L.; Heine, V. *Solid State Phys.* **1970**, *24*, 37.

0002-7863/92/1514-6466$03.00/0